Polymer Chemistry

ROYAL SOCIETY OF CHEMISTRY

PAPER

View Article Online
View Journal

Cite this: DOI: 10.1039/d5py00542f

Immunostimulatory pH-responsive nanogels derived from poly(oxanorbornene) precursor polymers†

Johannes Kockelmann and Lutz Nuhn *

Ring Opening Metathesis Polymerization (ROMP) provides access to well-defined poly(oxanorbornene) block copolymers that can be converted into micellar-derived immunoactive nanogels. We report on the synthesis of such immunoactive nanogels based on oxanorbornene-derived post-polymerization modification strategy. The key precursor, an oxanorbornene pentafluorophenyl ester (ONB-PFP) monomer, was synthesized and polymerized using living ring-opening metathesis polymerization (ROMP) facilitated by a third-generation Grubbs catalyst (G3) for efficient living-type block copolymerization. This approach yielded well-defined block copolymers by incorporating an active ester monomer with a hydrophilic triethylene glycol-functionalized oxanorbornene, establishing a robust platform for subsequent post-polymerization modifications. Nanogels were formed by aqueous self-assembly of the block copolymers, with various crosslinking agents employed to generate both acid-labile (D-NG) and non-degradable (ND-NG) nanogels, while without crosslinkers fully hydrophilic single polymer chains were obtained as controls. The covalent attachment of the Toll-like receptor 7/8 agonist IMDQ, an immunomodulatory imidazoquinoline agent, to the nanogels produced immunoactive nanogels, whose immunostimulatory efficacy was evaluated *in vitro* using a RAW-Blue macrophage reporter cell line. Flow cytometry confirmed efficient cellular uptake of only the intact nanogels by the macrophages resulting in a receptor activation and thus providing a strategy to safely control the delivery of the highly potent TLR7/8 agonist.

Received 2nd June 2025,
Accepted 18th July 2025

DOI: 10.1039/d5py00542f

rsc.li/polymers

Introduction

When hydrophobic polymers are used in drug delivery, insufficient shielding could lead to increased protein absorption and, therefore, non-specific cellular uptake.[1] To compensate for highly hydrophobic polymer backbones, *e.g.* the hydrocarbon backbone of poly(norbornene)s, the incorporation of highly hydrophilic side chains is necessary to enable sufficient solubility in water.[2,3] For improved biocompatibility and reduced non-specific interactions, less hydrophobic polymers are therefore recommended.[4,5] In analogy to previously investigated poly(meth acrylamide),[6–8] poly(norbornene)[2] and also poly(carbonate)[9] derived nanogels from our group, poly(oxanorbornene) nanogels are presented here as an alternative valuable polymeric platform for the preparation of stimuli responsive, immuno-activating nanogels, particularly relevant for cancer treatment.

Cancer immunotherapy focuses on the re-activation of the immune system against tumor cells. Naturally during cancer cell progression and subsequent invasion into the healthy tissue, the immune system generally recognizes and eliminates such malignant cells through the recognition of tumor-associated antigens. An immune evasion of cancer cells, however, occurs due to mainly four mechanisms:[10] (1) down-regulation of surface antigen expression, (2) upregulation of immune checkpoints, (3) recruitment of immune-suppressive cells (MDSCs, T_{reg}) and cytokines and (4) acidification of the tumor microenvironment. One strategy to boost anti-tumor immunogenicity is *via* reactivation of tumor-associated macrophages (TAMs) and dendritic cells (DCs).[11] For this, potent activators of the innate immune system, particularly Toll-like receptor agonists, have been developed, which subsequently reactivate TAMs and DCs. The potent TLR-7/8 agonist imidazoquinoline (IMDQ)[12] can be used for the reactivation of DCs or repolarization of immunosuppressive macrophage-phenotypes into immunoactive, tumoricidal phenotypes.[13,14] However, due to the poor pharmacological profile of this low molecular weight drug, its applied dose is limited due to the systemic activation of the immune system, causing in most cases fever, muscular weakness and fatigue syndromes.[15] The molecule rapidly distributes through the whole body.[16] Co-formulations of the

Chair of Macromolecular Chemistry, Center of Polymers for Life, Department of Chemistry and Pharmacy, Julius-Maximilians-Universität Würzburg, 97074 Würzburg, Germany. E-mail: lutz.nuhn@uni-wuerzburg.de

† Electronic supplementary information (ESI) available. See DOI: https://doi.org/10.1039/d5py00542f

TLR-agonist withing polymeric carriers offer a strategy to alter the pharmacokinetics and constrain the immune activity to draining lymph nodes and tumoral tissue.[6,8,16,17] To that respect, reactive-ester block copolymer derived nanogels have shown a valuable contribution to advance IMDQ's delivery into the lymphatic system.[7–9,16–18]

Previously, we investigated poly(norbornene) nanogels, which could control the delivery of IMDQ based on their structural integrity.[2] Despite their backbone hydrophobicity the polymeric norbornene chains could be solubilized with a 750 Da PEG-side chains and still allowed for the conjugation of the immunostimulatory small molecules.[2] Alternatively, more hydrophilic norbornenes would be attractive to reduce the PEG side chain density. To that respect, 7-oxanorbornene monomers are readily available alternatives for norbornene monomers. Their polymerization is easily achieved *via* ROMP and is generally similarly fast. High yields can be obtained as for norbornenes, too. The incorporation of an oxygen as a hydrogen-bond acceptor renders these polyether type polymers less hydrophobic than the norbornene derived polymers,[4,5,19] while their hydrophilicity can further be adjusted by short oligoethylene glycol side chains.[5] However, such polymers typically provide cloud point behavior which can be altered by the backbone chemistry, too. In analogy to methyacrylamide-based nanogels,[20] already smaller methoxy triethylene glycol side chains might then already be sufficient enough for 7-oxanorbornenes as hydrophilic species. A straightforward way for the covalent attachment of IMDQ to such polymeric carriers can then be achieved for 7-oxanorbornenes with active-ester side chains.[6,21] Especially pentafluorophenyl esters are desirable for post polymerization reactions because of their fast reaction kinetics during amidation reactions and relatively high resistance towards hydrolysis. The 7-oxanorbornene-2-carboxylic acid pentafluorophenyl ester was already described by Kiessling *et al.*[22,23] for the synthesis of carbohydrate-containing monomers *via* ROMP. However, a direct polymerization of this molecule by ROMP was not reported. As oxanorbornenes are typically well tolerated by metathesis catalysts and also exhibit enough ring strain for polymerization,[24] block copolymerization of 7-oxanorbornenes with methoxy triethylene glycol and pentafluorophenyl ester side chains offer a promising alternative route for the synthesis of functionalizable nanogels for a covalently attachment and controlled delivery of the highly potent TLR7/8 agonist IMDQ.

Results and discussion

Monomer synthesis

In general, norbornenes and oxanorbornenes can be synthesized *via* Diels–Alder reactions from furan (or cyclopentadiene) with suitable, mostly electron-poor olefines (see Fig. 1):

The 7-oxa-norbornene-2-carboxylic acid pentafluorophenyl ester ONB-PFP was synthesized in a three-step reaction sequence.[23,25] Starting from furan, the Diels–Alder reaction with acryloyl chloride afforded 7-oxanorbornene carboxylic

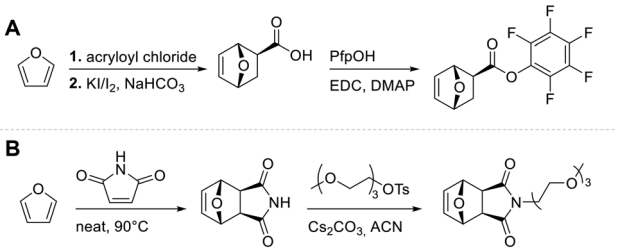

Fig. 1 (A) Synthesis of the PFP containing monomer ONB-PFP. (B) Synthesis of the triethylene glycol containing monomer ONB-TEG.

acid chloride as a 1 : 1.7 mixture of *endo* to *exo*-isomer. The acid chloride was then hydrolyzed with aqueous $NaHCO_3$ to yield the carboxylic acid. Generally, the *exo*-isomers of norbornenes and 7-oxanorbornenes are more reactive towards metathesis, due to less detrimental catalyst complexation. To remove the *endo* adduct and purify the more reactive *exo*-isomer,[26] an iodolactonization[22] of the *endo*/*exo* mixture and recrystallization of the crude product afforded the clean, crystalline 7-oxanorbornene-2-*exo*-carboxylic acid (Fig. S1†). In contrast to 5-norbornene-2-carboxylic acid, the oxanorbornene derivative is very soluble in water even at low pH, indicating a favorable higher hydrophilicity of the derived macromolecules compared to the norbornene analogue. The pentafluorophenyl ester was then synthesized *via* EDC coupling with pentafluorophenol.[23] To assess the stability of the monomer at room temperature, the retro-Diels–Alder reaction[22,27] was monitored *via* ^{1}H-NMR spectroscopy. The observed first order reaction rate constant and a corresponding reaction half-life of ~271 hours could be determined (Fig. S2†). The reaction is therefore sufficiently slow to easily handle the monomer at room temperature and to not compete with the very fast ROMP kinetics. The structure of the monomer as *exo* species could be carefully validated by ^{1}H,^{13}C-HSQC and ^{1}H,^{1}H-COSY NMR spectroscopy (Fig. S3†).

Polymerization

Homopolymerization. Next, the homopolymerization of both monomers was tested (see Fig. 2).

The reactivity of norbornenes and also (oxa)norbornenes towards ROMP is usually very high. This also applied to ONB-TEG and especially to ONB-PFP. At room temperature, the latter polymerized within seconds, and monomer conver-

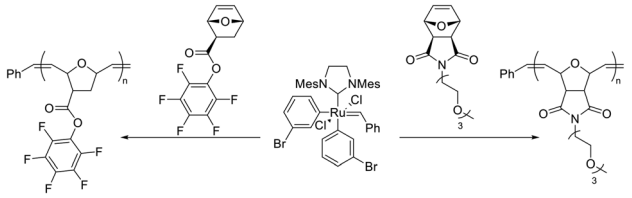

Fig. 2 ROMP of the monomers in the synthesis of homopolymers of ONB-PFP and ONB-TEG.

sion was usually quantitative. If the fast-initiating Grubbs third generation catalyst (G3) was used, the polymerization proceeded in a living-type fashion, as can be seen from the linear relationship of the number-average molecular weight (M_n) and the ratio of initial monomer concentration ($[M]_0$) to catalyst concentration ([Ru]) (Fig. 3 A1 and A2). To better attenuate the reactivity, the polymerizations were therefore performed at −20 °C. At higher temperatures, inhomogeneous initiation resulting in broader molecular weight dispersities was detected. Instead, at low temperatures the dispersities were usually very narrow which indicates uniform and fast monomer initiation.

The hydrophilic monomer ONB-TEG polymerized significantly slower than ONB-PFP. At −20 °C the initiation (indicated by the color change from bright green to orange/brown) took minutes, compared to seconds for ONB-PFP. Effective control over molecular weight could again be achieved by the G3 catalyst, too, as a linear correlation of M_n to M_0/Ru indicated once more living-type polymerization for the monomer (Fig. 3 B1 and B2). Remarkable, narrow molecular weight dispersities with $Đ < 1.2$ were monitored by size exclusion chromatography (SEC) for all polymers.

Metathesis derived polymers from norbornenes and oxanorbornenes can intrinsically be very heterogenous due to the double-bond stereochemistry, tacticity and connectivity in *C*1-symmetric monomers. The polymerization of an asymmetric monomer like ONB-PFP with the G3-catalyst therefore results in polymers with relatively broad and complex signals for the olefinic protons in their ^{1}H-NMR spectra (Fig. 3C). For the polymer derived from the symmetric monomer ONB-TEG, however, less differences in connectivities can occur and, therefore, also the proton spectrum becomes less complex (especially visible for the olefinic signals Fig. 3D). The splitting of signals in the olefinic region in the latter case is mostly determined by the *cis*/*trans* difference in the polymer backbone. For the ONB-PFP homopolymers, the *cis*/*trans* ratio of the double bonds can hardly be determined from the complex olefinic protons but better be derived from the allylic protons that provide a significant difference between *cis*- and *trans*-geometry. The almost equal *cis*/*trans* ratio in these polymers, for ONB-PFP, as well as for ONB-TEG (Tables S1 and S2†) confirms that under the applied conditions there is no specificity of double bond geometry during the polymerization with the G3-catalyst.[28]

The number-average degree of polymerization of the polymers can be determined from the ^{1}H-NMR spectra by integral analysis, involving a comparison between the phenyl-protons

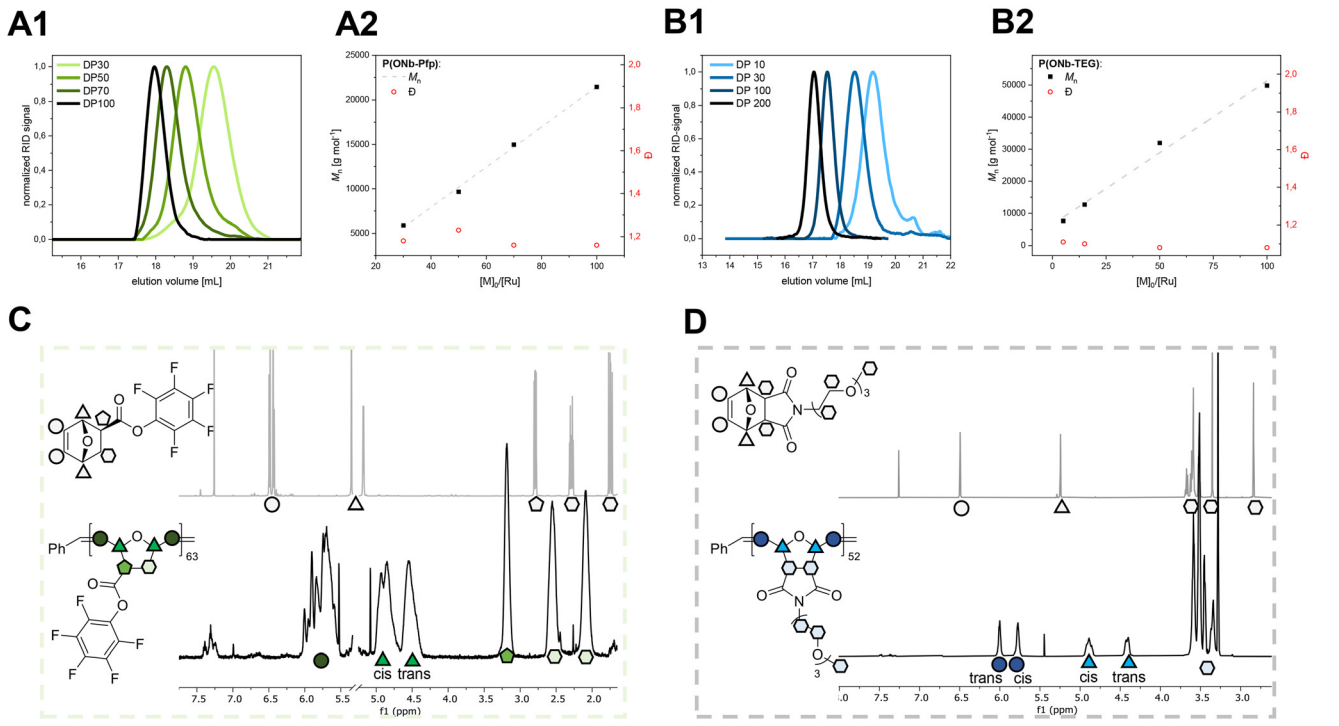

Fig. 3 (A1) SEC traces (HFIP, RID) of homopolymers of ONB-PFP prepared from different targeted molecular weights. (A2) Plot of the molecular weight (M_n), determined by SEC, against the ratio of initial monomer and catalyst concentration (M_0/Ru) for the homopolymers of ONB-PFP in black. The red circles depict the corresponding narrow dispersities ($Đ$). (B1) SEC traces (HFIP, RID) of homopolymers of ONB-TEG prepared from different targeted molecular weights. (B2) Plot of the molecular weight (M_n), determined by SEC, against the ratio of initial monomer and catalyst concentration (M_0/Ru) for the homopolymers of ONB-PFP in black. The red circles depict the corresponding dispersities. (C) Comparison of the ^{1}H-NMR spectra of ONB-PFP and poly(ONB-PFP) with the corresponding chemical structure and the signal assignments (for clarity, the solvent signal (CD_2Cl_2) is cut from the polymer spectrum). (D) Comparison of the ^{1}H-NMR spectra of ONB-TEG and poly(ONB-TEG) with the corresponding chemical structure and the signal assignment.

originating from the ruthenium initiator and the corresponding olefinic signals of the polymer. Coincidently, the solvent signal from CD_2Cl_2 does not impede the observation or analysis of either the olefinic signals or other signals of the polymers (Fig. 3C and D).

After polymerization the polymers were typically purified from the reaction mixture by three-times precipitations into hexane or diethyl ether. Noticeably, there was a little enhancement in polymer yields after precipitation with increasing molecular weights, which we assume is probably due to the increased solubility of smaller molecular weight fractions of the polymers in hexanes or diethyl ether.

Remarkably, when studying the water-solubility of ONB-TEG oxanorbornene polymers *versus* their norbornene analogues, an improved solubility was observed by a 10 °C higher cloud point (Fig. S7†), which corroborates our hypothesis of enhanced hydrophilicity for the poly(oxynorbornene)s than for the poly(norbornene)s.

Block copolymerization. After confirmation of successful living-type homopolymerization, a block copolymerization of ONB-PFP and ONB-TEG should be possible by sequential monomer addition. Similar to a previous poly(norbornene) system,[2] the block copolymerization sequence was designed to provide the hydrophobic phenyl unit to the solvophobic/hydrophobic block of the block copolymer. Consequently, ONB-PFP was polymerized first, followed by addition of the ONB-TEG monomer and polymerization onto the PFP-containing block. This approach allowed for the preparation of block copolymers with varying molecular weights. Analysis of the obtained materials was performed by HFIP SEC and ^{1}H-NMR spectroscopy.

For block copolymerization, G3 was dissolved in dry, degassed DCM and cooled to −20 °C. We favored again such lower temperatures resulting in slower initiation kinetics, as consequently lower $Đ$ values and a better control over the molecular weight could be achieved for the block copolymers, too. An appropriate amount of a stock solution of ONB-PFP was introduced to the cold catalyst solution in order to synthesize the first block. After 30 minutes and complete ONB-PFP monomer consumption determined by TLC, the second monomer (ONB-TEG) was added. When full monomer conversion was indicated by TLC, ethyl vinyl ether was added to liberate the catalyst from the polymer chain end and quench the polymerization. The block copolymers were then again three times precipitated from hexane. In this way various block copolymer lengths and compositions could be prepared, as summarized in Table 1.

The degree of polymerization was determined *via* ^{1}H-NMR by comparing the intensities of the phenyl-protons with a distinct set of protons of the PFP-block, while the TEG-block signals overlap with other signals of the PFP-block but can be derived from that, too (for detailed calculations compare Fig. S5†). DOSY-NMR (Fig. 4C and Fig. S4†) confirmed successful block copolymer formation, where only one single diffusing species is found providing ^{1}H-signals of all groups of the block copolymer.

Table 1 Summary of a selection of block copolymers from ONB-PFP and ONB-TEG

BP	ONB-PFP : ONB-TEG[a]	M_n[b] [kgmol^{-1}]	$Đ$[b]	Yield [%]
1	14 : 15	19.4	1.11	94
2	50 : 5	20.3	1.15	51
3	55 : 28	30.4	1.09	65
4	62 : 17	30.4	1.10	Quant.
5	58 : 38	42.4	1.14	76
6	240 : 30	56.3	1.26	80

[a] P_n of the individual blocks, determined *via* ^{1}H-NMR spectroscopy. [b] Determined *via* HFIP-SEC, PMMA-standard.

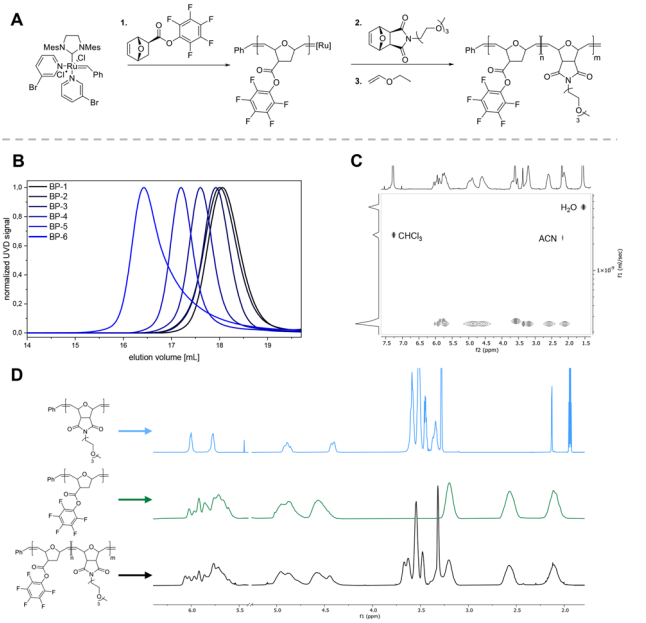

Fig. 4 (A) Reaction scheme for the block copolymerization of ONB-PFP and ONB-TEG with G3. (B) SEC-traces (HFIP, RID) of a selection of prepared block copolymers with different molecular weights and block compositions. (C) DOSY-NMR spectrum of a block copolymer showing the same diffusion constant for all block copolymer ^{1}H-signals. (D) Comparison of the NMR-spectra of the homopolymers and block polymer with distinct downfield signals for the PFP-containing block.

Nanogel synthesis

Next, poly(oxanorbornene) block copolymers were investigated for their self-assembly and sequential functionalization into core-crosslinked nanogels. Polymeric pentafluorophenyl esters have previously been shown to be insoluble in polar organic solvents like DMSO.[2,8,29] Self-assembly of the PFP-containing norbornene block polymers could therefore be observed in DMSO under anhydrous conditions. The ONB-PFP ester polymers are, however, at least in the low molecular weight regime sufficiently soluble in DMSO and, therefore, their derived block copolymers cannot self-assemble into particles. Only at higher degrees of polymerization, well defined particles could be obtained (BP6 – Fig. S8†). In most organic solvents (THF, acetone, $CHCl_3$, DCM), all block copolymers can be fully dis-

solved. Increasing polarity naturally decreases the solubility of the pentafluorophenylester block (DMSO > ethanol > methanol > water).[9] At a certain point, the block copolymers can then undergo microphase-separation and particles are formed. Also with other polymer systems, increased solubility in DMSO is observed, if the PFP-content is too low.[29,30]

Therefore, we had to test several alternative solvents for self-assembly of the oxanobornene block copolymers. First studies with alcohols revealed that direct solubilizations were not feasible. However, by slow evaporation of acetone from an aqueous solution the aggregation of the block copolymers into polymeric particles could be achieved successfully. Under these conditions, enough mobility could be assured for block copolymers in solution, while the solvent polarity gradually increased allowing the PFP-ester block to microphase-separate and self-assemble into block copolymers in a controlled way. Remarkably, under the applied conditions the hydrolysis of the pentafluorophenyl esters was rather slow, which is probably due to suppressed water diffusion into the hydrophobic pentafluorophenyl ester containing core. This goes along well with studies on hydrophilic tetrafluorophenyl esters in water whose hydrolyses were reported to be relatively slow, too.[31] Only at elevated temperatures significant ester hydrolysis needs to be considered.[32] Under the applied conditions, however, our observations could exclude any detectable PFP-ester hydrolysis during nanogel syntheses by ^{19}F NMR spectroscopy (Fig. S9†).

Next, the PFP-esters inside the micelles were used for subsequent crosslinking, functionalization and hydrophilization (Fig. 5A). For that purpose, we first added either a ketal-containing bisamine or an ether-containing bisamine for crosslinking affording degradable (D-NG) or non-degradable nanogels (ND-NG), respectively (by ^{19}F NMR spectroscopy a release of pentafluoropheny could be found immediately upon addition of 2,2′-(ethylendioxy)-diethylamine – Fig. S9†). To ensure full conversion of the PFP-esters and to further hydrophilize the resulting crosslinked particles, a hydrophilic methoxy triethylene glycol amine was added in excess. The resulting reaction mixture was then dialyzed against water to remove the liberated pentafluorophenol, the base catalyst and excess amines. After lyophilization the purified nanogel particles could be obtained as voluminous powders. They could be readily re-dispersed again into water or buffer for subsequent applications.

We tested several polymers for their aggregation behavior and nanogel formation. The results of the nanogel formation are summarized in Table S4.† The size of the nanogels is typically determined by the size of the self-assembled block copolymer micelles (Fig. S11†). A direct correlation between block copolymer composition and nanogel size could not be derived,

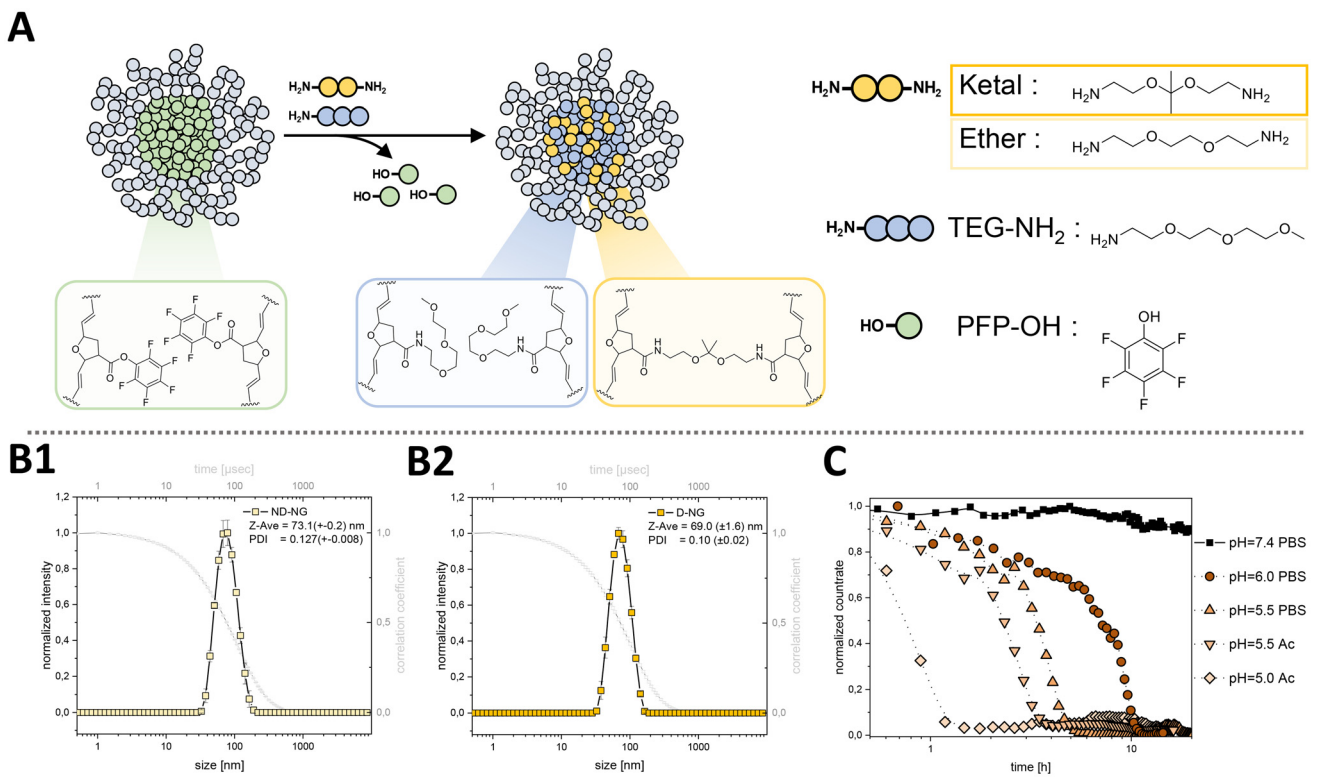

Fig. 5 (A) Schematic overview of the sequential nanogel formation from ONB-PFP derived block copolymer micelles in water. Depending on the crosslinker, degradable (ketal) and non-degradable (ether) particles can be prepared. (B1) DLS distribution of non-degradable, ether crosslinkers nanogels (ND-NG). (B2) DLS distribution of degradable, ketal crosslinked nanogels (D-NG). (C) Particle degradation, measured by DLS at different pH values in respective buffers.

as for the norbornene nanogels.[2] We hypothesize that the altered reaction conditions including water as solvent make it rather challenging to access the thermodynamically most favorable micelle structures prior to crosslinking. Nonetheless, the probably kinetically entrapped polymer aggregates can reproducibly be converted into the affording nanogels of similar sizes (Fig. S5†). To yield particles with sizes around 70 nm, we therefore applied polymers with similar molecular weights and block compositions as for BP-3 (Table S4†).

DLS measurements further confirmed that the sizes of the resulting nanogels were independent from their crosslinker. The ketal-containing bisamine crosslinker 2,2-bis(aminoethoxy)propane served as pH-degradable crosslinker, while the ether-containing bisamine crosslinker 2,2′-(ethylenedioxy)-diethylamine served as non-degradable crosslinker. For both resulting pH-degradable and non-degradable nanogels (D-NG and ND-NG) uniform particles with sizes of around 70 nm were obtained (Fig. 5B). To analyze the pH-responsive behavior, DLS measurements of the D-NG were recorded in various buffer solutions of decreasing pH-values over time (Fig. 5C). The kinetics of ketal hydrolysis were proven by decreasing scattering intensities and complete nanogel degradation was achieved within 10 hours at pH 6. For lower pH-values like pH = 5 faster degradations occurred within 1 hour, whereas at physiological pH = 7.4 the nanogels remained fully stable. This is in agreement with previous degradation studies of nanogels with ketal-containing crosslinkers.[2,8,18]

FRET measurements. The reactive ester approach allows for covalent functionalization of the nanogels by addition of mono-amine functionalizes species. For instance, fluorescent dye labelling can straightforwardly be achieved by adding the respective fluorophores carrying a single primary amine. These features can also be applied to investigate particle integrity *via* Förster-Resonance-Energy-Transfer (FRET) when the individual block copolymer chains have before been labeled with Cy3 and Cy5. Only when both dyes are in close proximity, an efficient transfer of energy can occur from the electronically excited Cy3-donor dye to the Cy5-acceptor, affording a Cy5 emission upon Cy3 excitation. The efficiency of this energy transfer is strongly dependent on the distance between those two molecules. In the nanogel setup, an acid-triggered ketal hydrolysis would afford disassembly of the Cy3- and Cy5-labeled polymers leading to a decrease in energy transfer and reduction of Cy5 emission upon Cy3 excitation.

Fig. 6A illustrates the synthetic scheme for preparing such FRET particles. Initially, the block copolymers were individually functionalized with either Cy3 amine or Cy5 amine, yielding the respective single dye-labeled block copolymers (Fig. S6†). Equal amounts of these block copolymers were then used to provide either degradable nanogels with ketal-crosslinks or non-degradable nanogels with ether-crosslinks. Similar to the synthesis described above, the remaining pentafluorophenyl esters were again quenched with an excess of triethylene glycol amine to ensure complete removal of pentafluorophenol and hydrophilization of the crosslinked polymers. The resulting FRET-nanogels were analyzed by UV–Vis and fluorescence emission spectroscopy in various buffers. For the FRET measurements, samples were excited at 490 nm and their emission spectra recorded. The fluorescence intensities at 565 nm (corresponding to the Cy3 FRET donor) and 666 nm (corresponding Cy5 FRET acceptor) were compared to determine the FRET ratio. This could be monitored over time under varying pH conditions (Fig. 6B).

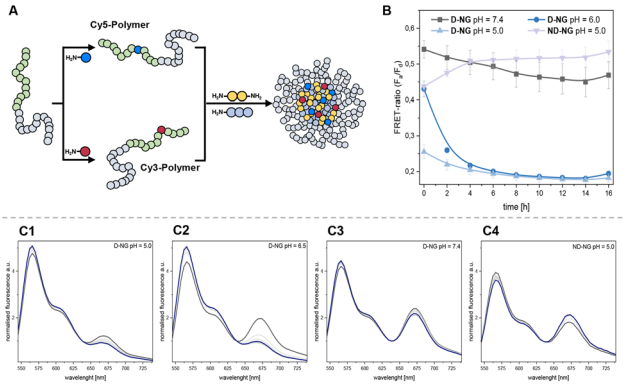

Fig. 6 (A) Scheme for the synthesis of both Cy5- and Cy3-containing poly(oxanorbornene) block copolymers and the synthesis of Cy5- and Cy3-labeled nanogels. (B) Plot of the FRET-ratio against time for the ketal-crosslinked FRET-nanogel at different pH-values. (C1–4) Corresponding fluorescence emission spectra at different pH-values for the ketal-crosslinked and the ether-crosslinked nanogel.

In the fluorescence emission spectra displayed in Fig. 6 C1–C3 an immediate decrease in fluorescence intensity at 666 nm could be found pH = 5, while at pH = 6 there was still some initiation fluorescence at 666 nm that disappeared while the donor fluorescence at 565 nm increased. At physiological pH = 7.4 a suppressed donor fluorescence at 565 nm and a stable acceptor fluorescence emission at 666 nm remain constant. When calculating the respective FRET ratios at the given time points (Fig. 6B), the measurements of the degradable nanogels confirm again its relative stability at pH = 7.4 and are in accordance with the DLS results over time at the same pH-value (Fig. 5C). However, already at pH 6.0, the FRET ratio drops to a minimum value of approximately 0.2 within 6 hours. The decrease is even more rapid at pH 5.0 (a pH value that is typically reached for nanoparticles internalized by cellular endolysosomal uptake pathways[33]). The fast kinetics of the hydrolysis are also supported by comparing them with the decrease in scattered light intensity for the ketal-containing D-NG in Fig. 5C. In contrast, ether-crosslinked particles exhibit relatively high FRET ratios that remain stable even at pH 5.0 after several hours. Altogether, these observations confirm that fluorescent dye labeling of the nanogels with primary amines is a valuable tool not only for tracing the particles but also confirming their integrity.

This could be further demonstrated by first uptake studies *in vitro*. RAW-Blue macrophages as relevant phagocytosing immune cells were incubated with the single- or dual-labeled nanogels for 4 hours at 37 °C and then characterized by flow cytometry. Upon excitation at 488 nm the emission of the Cy3

label as well as the FRET-induced Cy5 emission could be detected with individual flow cytometry channels. Besides, upon excitation at 633 nm the emission of the Cy5 label could be recorded, too (Fig. S19†). Interestingly, for the dual-labeled ether-crosslinked nanogel a reduced signal was recorded for the Cy3 emission (Fig. S19A†), while its FRET emission was still high in opposite to the ketal-crosslinked nanogel (Fig. S19C†), which provided a stronger Cy3 emission (Fig. S19A†). When again forming the FRET ratio from the two channels, a threefold higher FRET ratio was derived for the ether-crosslinked nanogels than for the ketal-crosslinked nanogels (Fig. S19D†), indicating their robust integrity of the ether-crosslinked nanogels *versus* the ketal-crosslinked nanogels which suggest an immediate intracellular ketal hydrolysis.[37,38]

IMDQ-conjugation for the preparation of immune active nanogels

In analogy to the prepared FRET nanogels by dye labelling with Cy3 and Cy5, the reactive ester oxanorbornene block copolymers were also utilized for the covalent conjugation of the small-molecule TLR7/8 agonist imidazoquinoline (IMDQ). IMDQ was selected due to its nanomolar potency in TLR7/8 activation of antigen-presenting cells (*e.g.* dendritic cells, macrophages) and its promising performance in *in vivo* immunostimulation studies for vaccination purposes.[7–9] The ligation of IMDQ together with another fluorophore, tetramethyl rhodamine cadaverine (TAMRA), could be performed because these molecules provided a single primary amine that allows for selective conjugation to the PFP-esters.[13] Similar to the empty nanogels, TAMRA and IMDQ conjugation was performed by adding the free amines to a solution of PFP-ester containing block copolymers, which had already been preassembled into block copolymer micelles. Followed by bisamine crosslinking and hydrophilization with methoxy triethylene glycol amine, drug and dye loaded nanogel particles could be isolated after dialysis (note that also a non-crosslinked soluble polymer species could be obtained when no crosslinker was added but all precursor block copolymers was then quenched by methoxy triethylene glycol amine). The conjugation efficiency of IMDQ was determined by UV–Vis spectroscopy and the absorbance compared to the nanogels only loaded with TAMRA but without IMDQ. Consequently, a mass-fraction of IMDQ was determined of around 10–13 wt% of drug loading (Fig. S12†). The size of the dye-labeled nanogels with or without IMDQ was verified by DLS, and revealed for the crosslinked nanogels in both cases particles with similar diameters of below 70 nm (Fig. S13 and S14† – for the non-crosslinked polymers lower correlations and count rates could be found by DLS that indicated individually diffusing polymer chains when no IMDQ was conjugated). In conclusion, the multiple covalent drug and dye conjugation did again obviously not affect the size of the nanogels derived from the self-assembled oxanorbornene precursor polymers.

The both drug and dye loaded particles could be again be investigated for their intracellular uptake again into phagocytosing immune cells as relevant targets for IMDQ delivery. For that purpose, RAW-Blue macrophages were incubated with both degradable (D-NG) and non-degradable (ND-NG) TAMRA-labeled nanogels, comprising both IMDQ-conjugated and unconjugated variants. Similarly, the non-crosslinked polymers, with and without IMDQ conjugation, were evaluated, too. Incubation of RAW-Blue cells with the respective materials was allowed for 24 hours, after which measurements were conducted by flow cytometry analysis (Fig. S16 and S17†). Remarkably, the IMDQ-conjugated versions of all three types of conjugates exhibited significantly enhanced cellular uptake compared to their IMDQ-free counterparts (Fig. 7C and D and Fig. S18†). Of particular interest was the notably poor uptake of non-crosslinked polymers by macrophages (Fig. 7C and D). This is in analogy to previous reports on poly(methacrylamide)-based nanogels[8,17] where a similar poor uptake was found for the soluble polymers *versus* the cross-linked nanogels, too.

For quantification of the TLR-7/8 stimulation activity, the RAW-Blue macrophages were finally investigated for their reporter function. The cell line is genetically engineered to monitor activation of the NFκB-pathway upon pattern recognition receptor (*e.g.* TLR7/8) stimulation by secretion of soluble alkaline phosphatase. The amount of phosphatase can then be detected by a photometric assay (Quanti Blue). Activation of NFκB-pathway has been demonstrated to correlate well with *in vivo* immunostimulation and was therefore taken as marker for efficient activation of macrophages.[7–9,34] For that purpose, the cells were incubated with increasing amounts of IMDQ, either in soluble form or attached to the nanogels (D-NG, ND-NG, or P). In parallel, the viability of RAW-blue cells could be evaluated by MTT-assay, too (Fig. S15†). Neither the IMDQ-conjugated nor the empty nanocarriers showed significant influence on the cell viability up to 60–80 mg L^{-1}. However, full confirmation of biocompatibility would require further investigation, as the MTT assay provides only a preliminary indication of cytotoxicity and is by no means comprehensive. When looking at the immune activation capabilities, different results were obtained for D-NG and ND-NG than for the non-crosslinked P (Fig. 7B). As expected, the empty nanogels and polymers do not show any TLR-activation, while soluble unconjugated IMDQ triggered the TLR-activation most effectively, even at sub-micromolar concentrations (EC_{50} ~0.03 μm). D-NG, and ND-NG, covalently carrying the IMDQ, provided a TLR stimulation activity at increasing doses in the micromolar regime. The apparent EC_{50} of the conjugated IMDQ was around ~12 μm for D-NG and ~16 μm for ND-NG (such decrease in activity compared to the soluble IMDQ has been observed also for other covalent nanoparticulate formulations of IMDQ,[9,18,35,36] albeit not as pronounced). Interestingly, the non-crosslinked polymers, conjugated to IMDQ did not induce any comparable activation of TLR7/8 at these concentrations. No activity could be detected in the concentration ranges, tested in this study. This finding has previously also been observed with poly(norbornene nanogels)[2] and is also noticed, when IMDQ is conjugated to highly

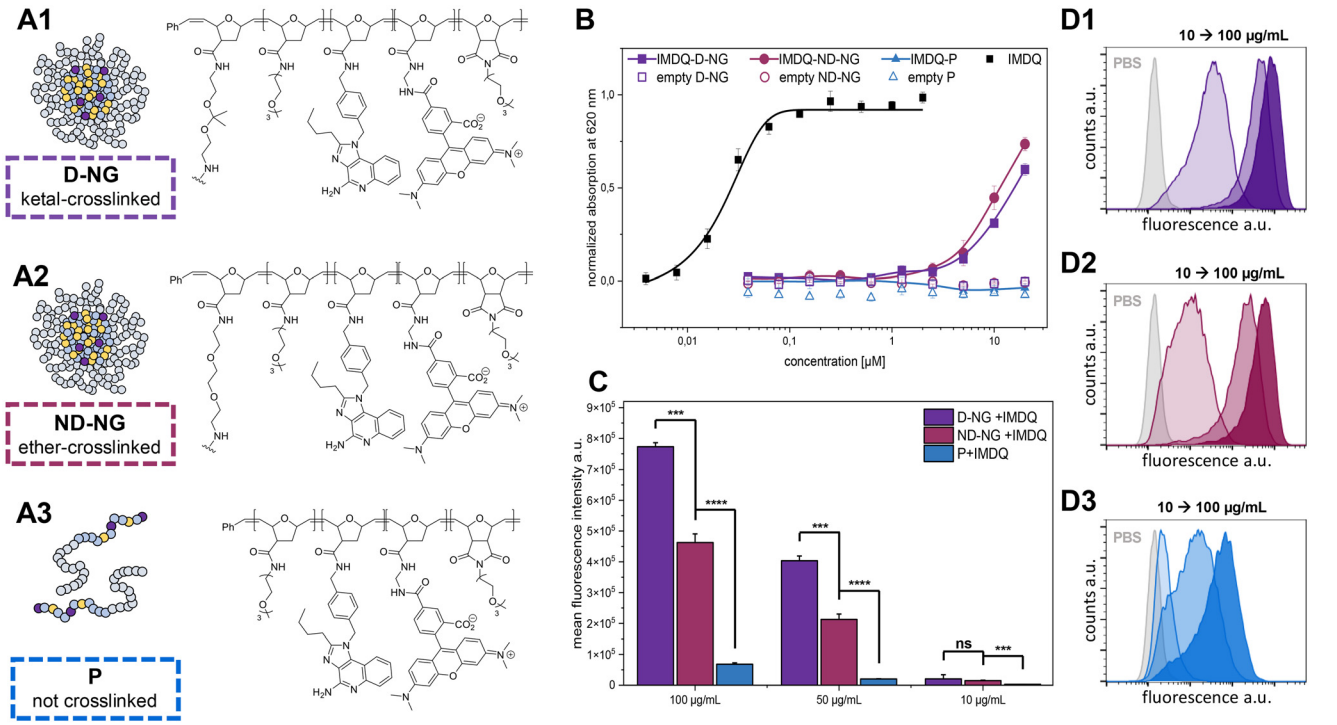

Fig. 7 Upkate and TLR 7/8 receptor stimulation of nanogels and polymers derived from self-assembeld oxanorbornene precursor block copolymers. (A) Structures of the investigated crosslinked nanogels (A1–2) and polymers (A3). (B) Results of the TLR 7/8 activation in RAW-Blue macrophage recporter cells, treated with poly(oxanorbornene)-derived imidazoquinoline nanocarriers (n = 4). (C) Quantitative analysis of mean fluorescence intensities derived from the flow cytometry measurements of RAW-Blue macrophages treated with poly(oxanorbornene)-derived imidazoquinoline nanocarriers (n = 3, ns: $p > 0.05$, *: $p \leq 0.05$, **: $p \leq 0.01$, ***: $p \leq 0.001$, ****: $p \leq 0.0001$). (D1–3) Flow cytometry histograms of RAW-Blue macrophages treated with TAMRA-labeled poly(oxa)norbornene derived imidazoquinoline nanocarriers (n = 3).

hydrophilic PEG-chains.[36] We speculate that the decreased activity is likely due to a significantly reduced uptake of non-crosslinked polymer chains (Fig. 7D).

In previous studies involving poly(norbornene) nanogels, flow cytometry uptake studies revealed comparable uptake behavior for both nanogels and polymers, suggesting that different uptake mechanisms might account for the diminished activity observed with non-crosslinked polymers. Our current study, however, now reveals differing uptake properties between polymers and nanogels; the non-crosslinked polymers are taken up by macrophages much less efficiently than the nanogels. This reduced uptake implies that the polymers exhibit weaker immune activation due to their more hydrophilic nature, resulting in less interaction with the cells. This also implies again an advantageous delivery property of this carrier system, as only intact nanogels are able to effectively trigger innate immune cell TLR 7/8 receptor activation of their covalently attached agonist payload.

Conclusions

In summary, we have explored for the first time the use of novel oxanorbornene block copolymers for the preparation of immunoactive nanogels. The pentafluorophenyl ester-containing oxanorbornene monomer (ONB-PFP) and the water-soluble methoxy triethylene glycol containing oxanorbornene monomer (ONB-TEG) could be polymerized using the G3-catalyst, achieving a successful living polymerization process. The pentafluorophenyl ester is ideal for subsequent post-polymerization modifications. This method enabled the creation of well-defined homopolymers and block copolymers.

The nanogels were prepared using the triethylene glycol-containing block copolymers in an aqueous environment, notably without any detectable hydrolysis of the active ester. By employing different crosslinkers, we were able to produce both acid-labile ketal nanogels (D-NG) and non-degadable ether nanogels (ND-NG), as well as non-crosslinked, hydrophilic polymer variants. The degradability of the nanogels was investigated with dynamic light scattering and FRET-measurements *via* Cy3 and Cy5 precursor polymer labelled particles. In general, the synthesis of both poly(oxa)norbornenes and poly(norbornene)s is highly reproducible, yielding well-defined homo- and block copolymers. The more hydrophilic nature of the poly(oxanorbornene) backbone, however, would allow for higher covalent drug loadings with hydrophobic drugs, while still enabling efficient nanogel ketal degradation and unfolding into fully soluble single polymer chains in water.

Further, the covalent conjugation of the immunostimulatory TLR 7/8 agonist IMDQ to the nanogels could be investigated, too, resulting in the formation of immunoactive nanogels. The immunoactivity of these nanogels was tested *in vitro*

using the RAW-Blue reporter cell line. Here, a drastic significant difference in both cellular-uptake and TLR-activation was observed for the nanogels, in comparison with their non-crosslinked polymers representing the degradation products of the ketal-crosslinked nanogels. In addition, it would be interesting to compare different TLR 7/8 agonists either by further hydrophobic encapsulation (*e.g.* Adifectin, CL075 *etc.*)[39] or by covalently attaching such ligands either directly to the nanogels or *via* cleavable linkers.[3] Utilizing cationic crosslinkers (spermine) would also allow for an electrostatically driven encapsulation of oligonucleotides as potent TLR9 agonists like the CpG sequence, as earlier demonstrated.[34,40] In comparison to the highly PEGylated polynorbornene nanogels,[2] the oxanorbornene-derived nanogels, with lower degree of PEGylation, exhibited significantly higher cellular uptake. This behavior can be attributed to the inherently higher hydrophilicity of the oxanorbornene backbone, which allowed for reduced PEG content without compromising aqueous stability. The loss of cell uptake and TLR-activation represents a valuable feature that controls the safety profile of the agonist by the poly(oxanorbornene)-derived nanogels.

Conflicts of interest

There are no conflicts to declare.

Data availability

All data supporting this article have been included as part of the ESI.†

Acknowledgements

The authors want to gratefully acknowledge financial support by the DFG through the Emmy Noether program, the SFB 1066 (project B03 and B04) and the TRR 225 (project B05).

References

1 (*a*) J. Simon, T. Wolf, K. Klein, K. Landfester, F. R. Wurm and V. Mailänder, *Angew. Chem., Int. Ed.*, 2018, **57**, 5548; (*b*) M. Li, S. Jiang, J. Simon, D. Paßlick, M.-L. Frey, M. Wagner, V. Mailänder, D. Crespy and K. Landfester, *Nano Lett.*, 2021, **21**, 1591.
2 J. Kockelmann, J. Stickdorn, S. Kasmi, J. de Vrieze, M. Pieszka, D. Y. W. Ng, S. A. David, B. G. de Geest and L. Nuhn, *Biomacromolecules*, 2020, **21**, 2246.
3 S. H. Bhagchandani, F. Vohidov, L. E. Milling, E. Y. Tong, C. M. Brown, M. L. Ramseier, B. Liu, T. B. Fessenden, H. V.-T. Nguyen, G. R. Kiel, *et al.*, *Sci. Adv.*, 2023, **9**, eadg2239.
4 K. Lienkamp, C. F. Kins, S. F. Alfred, A. E. Madkour and G. N. Tew, *J. Polym. Sci., Part A:Polym. Chem.*, 2009, **47**, 1266.
5 S. F. Alfred, Z. M. Al-Badri, A. E. Madkour, K. Lienkamp and G. N. Tew, *J. Polym. Sci., Part A:Polym. Chem.*, 2008, **46**, 2640.
6 J. Stickdorn and L. Nuhn, *Eur. Polym. J.*, 2020, **124**, 109481.
7 J. Stickdorn, L. Stein, D. Arnold-Schild, J. Hahlbrock, C. Medina-Montano, J. Bartneck, T. Ziß, E. Montermann, C. Kappel, D. Hobernik, *et al.*, *ACS Nano*, 2022, **16**, 4426.
8 L. Nuhn, N. Vanparijs, A. de Beuckelaer, L. Lybaert, G. Verstraete, K. Deswarte, S. Lienenklaus, N. M. Shukla, A. C. D. Salyer, B. N. Lambrecht, *et al.*, *Proc. Natl. Acad. Sci. U. S. A.*, 2016, **113**, 8098.
9 C. Czysch, C. Medina–Montano, Z. Zhong, A. Fuchs, J. Stickdorn, P. Winterwerber, S. Schmitt, K. Deswarte, M. Raabe, M. Scherger, *et al.*, *Adv. Funct. Mater.*, 2022, **32**, 2203490.
10 C. Liu, M. Yang, D. Zhang, M. Chen and D. Zhu, *Front. Immunol.*, 2022, **13**, 961805.
11 S. Gallucci, M. Lolkema and P. Matzinger, *Nat. Med.*, 1999, **5**, 1249.
12 M. Beesu, A. C. D. Salyer, M. J. H. Brush, K. L. Trautman, J. K. Hill and S. A. David, *J. Med. Chem.*, 2017, **60**, 2084.
13 E. Bolli, M. Scherger, S. M. Arnouk, A. R. Pombo Antunes, D. Straßburger, M. Urschbach, J. Stickdorn, K. De Vlaminck, K. Movahedi, H. J. Räder, *et al.*, *Adv. Sci.*, 2021, **8**, 2004574.
14 (*a*) L. A. J. O'Neill, D. Golenbock and A. G. Bowie, *Nat. Rev. Immunol.*, 2013, **13**, 453; (*b*) A. Iwasaki and R. Medzhitov, *Nat. Immunol.*, 2015, **16**, 343; (*c*) M. P. Schön and M. Schön, *Oncogene*, 2008, **27**, 190; (*d*) R. J. Mancini, L. Stutts, K. A. Ryu, J. K. Tom and A. P. Esser-Kahn, *ACS Chem. Biol.*, 2014, **9**, 1075.
15 (*a*) B. J. Weigel, S. Cooley, T. DeFor, D. J. Weisdorf, A. Panoskaltsis-Mortari, W. Chen, B. R. Blazar and J. S. Miller, *Am. J. Hematol.*, 2012, **87**, 953; (*b*) A. Z. Dudek, C. Yunis, L. I. Harrison, S. Kumar, R. Hawkinson, S. Cooley, J. P. Vasilakos, K. S. Gorski and J. S. Miller, *Clin. Cancer Res.*, 2007, **13**, 7119.
16 L. Nuhn, S. de Koker, S. van Lint, Z. Zhong, J. P. Catani, F. Combes, K. Deswarte, Y. Li, B. N. Lambrecht, S. Lienenklaus, *et al.*, *Adv. Mater.*, 2018, **30**, e1803397.
17 L. Nuhn, L. van Hoecke, K. Deswarte, B. Schepens, Y. Li, B. N. Lambrecht, S. de Koker, S. A. David, X. Saelens and B. G. de Geest, *Biomaterials*, 2018, **178**, 643.
18 A. Huppertsberg, L. Kaps, Z. Zhong, S. Schmitt, J. Stickdorn, K. Deswarte, F. Combes, C. Czysch, J. de Vrieze, S. Kasmi, *et al.*, *J. Am. Chem. Soc.*, 2021, **143**, 9872.
19 S. F. Alfred, K. Lienkamp, A. E. Madkour and G. N. Tew, *J. Polym. Sci., Part A:Polym. Chem.*, 2008, **46**, 6672.
20 L. Nuhn, M. Hirsch, B. Krieg, K. Koynov, K. Fischer, M. Schmidt, M. Helm and R. Zentel, *ACS Nano*, 2012, **6**, 2198.
21 A. Das and P. Theato, *Chem. Rev.*, 2016, **116**, 1434.
22 D. D. Manning, L. E. Strong, X. Hu, P. J. Beck and L. L. Kiessling, *Tetrahedron*, 1997, **53**, 11937.
23 C. M. Schueller, D. D. Manning and L. L. Kiessling, *Tetrahedron Lett.*, 1996, **37**, 8853.

24 J. Howell, J. D. Goddard and W. Tam, *Tetrahedron*, 2009, **65**, 4562.
25 F. Sinner and M. R. Buchmeiser, *Macromolecules*, 2000, **33**, 5777.
26 (*a*) J. M. Pollino, L. P. Stubbs and M. Weck, *Macromolecules*, 2003, **36**, 2230; (*b*) M. G. Hyatt, D. J. Walsh, R. L. Lord, J. G. Andino Martinez and D. Guironnet, *J. Am. Chem. Soc.*, 2019, **141**, 17918.
27 V. Froidevaux, M. Borne, E. Laborbe, R. Auvergne, A. Gandini and B. Boutevin, *RSC Adv.*, 2015, **5**, 37742.
28 J.-A. Song, G. I. Peterson, K.-T. Bang, T. S. Ahmed, J.-C. Sung, R. H. Grubbs and T.-L. Choi, *J. Am. Chem. Soc.*, 2020, **142**, 10438.
29 N. Leber, L. Nuhn and R. Zentel, *Macromol. Biosci.*, 2017, **17**, 1700092.
30 B. Couturaud, P. G. Georgiou, S. Varlas, J. R. Jones, M. C. Arno, J. C. Foster and R. K. O'Reilly, *Macromol. Rapid Commun.*, 2019, **40**, e1800460.
31 (*a*) J. Charoenpattarapreeda, Y. S. Tan, J. Iegre, S. J. Walsh, E. Fowler, R. S. Eapen, Y. Wu, H. F. Sore, C. S. Verma, L. Itzhaki, *et al.*, *Chem. Commun.*, 2019, **55**, 7914; (*b*) K. R. Gee, E. A. Archer and H. C. Kang, *Tetrahedron Lett.*, 1999, **40**, 1471; (*c*) S. Tsuji, K. Kobayashi, T. Fujii, H. Imoto, K. Naka, Y. Aso, H. Ohara and T. Tanaka, *Macromol. Chem. Phys.*, 2022, **223**, 2200072.
32 N. Mohr, M. Barz, R. Forst and R. Zentel, *Macromol. Rapid Commun.*, 2014, **35**, 1522.
33 S. Ohkuma and B. Poole, *Proc. Natl. Acad. Sci. U. S. A.*, 1978, **75**, 3327.
34 A. Fuchs, C. Czysch, K. Maxeiner, P. Winterwerber, S. Schmitt, J. Stickdorn, Z. Zhong, C. Medina-Montano, H.-J. Räder, M. Bros, *et al.*, *Small*, 2024, e2406082.
35 (*a*) M. Tang, B. Chen, H. Xia, M. Pan, R. Zhao, J. Zhou, Q. Yin, F. Wan, Y. Yan, C. Fu, *et al.*, *Nat. Commun.*, 2023, **14**, 5888; (*b*) A. A. A. Smith, E. C. Gale, G. A. Roth, C. L. Maikawa, S. Correa, A. C. Yu and E. A. Appel, *Biomacromolecules*, 2020, **21**, 3704.
36 B. Wang, S. van Herck, Y. Chen, X. Bai, Z. Zhong, K. Deswarte, B. N. Lambrecht, N. N. Sanders, S. Lienenklaus, H. W. Scheeren, *et al.*, *J. Am. Chem. Soc.*, 2020, **142**, 12133.
37 L. Nuhn, S. Van Herck, A. Best, K. Deswarte, M. Kokkinupoulou, I. Lieberwirth, K. Koynov, B. N. Lambrecht and B. G. De Geest, *Angew. Chem., Int. Ed.*, 2018, **57**, 10760.
38 B. Louage, M. J. Van Steenbergen, L. Nuhn, M. D. P. Risseeuw, I. Karalic, J. Winne, S. Van Calenbergh, W. E. Hennink and B. G. De Geest, *ACS Macro Lett.*, 2017, **6**, 272.
39 (*a*) L. Bixenmann, J. Stickdorn and L. Nuhn, *Polym. Chem.*, 2020, **11**, 2441; (*b*) C. Czysch, C. Medina-Montano, N.-J. K. Dal, T. Dinh, Y. Fröder, P. Winterwerber, K. Maxeiner, H.-J. Räder, D. Schuppan, H. Schild, M. Bros, B. Biersack, F. Fenaroli, S. Grabbe and L. Nuhn, *Macromol. Rapid. Commun.*, 2022, **45**, 2200095; (*c*) L. Bixenmann, T. Ahmad, F. Stephan and L. Nuhn, *Biomacromolecules*, 2024, **25**, 7958; (*d*) A. V. Hauck, P. Komforth, J. Erlenbusch, J. Stickdorn, K. Radacki, H. Braunschweig, P. Besenius, S. Van Herck and L. Nuhn, *Biomater. Sci.*, 2025, **13**, 1414; (*e*) L. Bixenmann, A. V. Hauck, T. Ahmad and L. Nuhn, *Macromolecules*, 2025, **58**, 2879.
40 S. Hartmann, L. Nuhn, B. Palitzsch, M. Glaffig, N. Stergiou, B. Gerlitzki, E. Schmitt, H. Kunz and R. Zentel, *Adv. Healthcare Mater.*, 2014, **4**, 522.

